OPEN

Noncontact Phased-Array Ultrasound Facilitates Acute Wound Healing in Mice

Nao Wakabayashi, M.D.
Atsushi Sakai, Ph.D.
Hiroya Takada, Ph.D.
Takayuki Hoshi, Ph.D.
Hitomi Sano, M.D., Ph.D.
Shizuko Ichinose, Ph.D.
Hidenori Suzuki, M.D., Ph.D.
Rei Ogawa, M.D., Ph.D.

Tokyo, Japan

Background: The authors developed a noncontact low-frequency ultrasound device that delivers high-intensity mechanical force based on phased-array technology. It may aid wound healing because it is likely to be associated with lower risks of infection and heat-induced pain compared with conventional ultrasound methods. The authors hypothesized that the microdeformation it induces accelerates wound epithelialization. Its effects on key wound-healing processes (angiogenesis, collagen accumulation, and angiogenesis-related gene transcription) were also examined.

Methods: Immediately after wounding, bilateral acute wounds in C57BL/6J mice were noncontact low-frequency ultrasound– and sham-stimulated for 1 hour/day for 3 consecutive days (10 Hz/90.6 Pa). Wound closure (epithelialization) was recorded every 2 days as the percentage change in wound area relative to baseline. Wound tissue was procured on days 2, 5, 7, and 14 (five to six per time point) and subjected to histopathology with hematoxylin and eosin and Masson trichrome staining, CD31 immunohistochemistry, and quantitative polymerase-chain reaction analysis.

Results: Compared to sham-treated wounds, ultrasound/phased-array–treated wounds exhibited significantly accelerated epithelialization (65 ± 27 percent versus 30 ± 33 percent closure), angiogenesis (4.6 ± 1.7 percent versus 2.2 ± 1.0 percent $CD31^+$ area), and collagen deposition (44 ± 14 percent versus 28 ± 13 percent collagen density) on days 5, 2, and 5, respectively (all $p < 0.05$). The expression of Notch ligand delta-like 1 protein (Dll1) and Notch1, which participate in angiogenesis, was transiently enhanced by treatment on days 2 and 5, respectively.

Conclusions: The authors' noncontact low-frequency ultrasound phased-array device improved the wound-healing rate. It was associated with increased early neovascularization that was followed by high levels of collagen-matrix production and epithelialization. The device may expand the mechanotherapeutic proangiogenesis field, thereby helping stimulate a revolution in infected wound care. (*Plast. Reconstr. Surg.* 145: 348e, 2020.)

Over the past few decades, negative-pressure wound therapy (also known as microdeformational wound therapy) has revolutionized the treatment of complex wounds. It involves aspiration of noninfected wounds by a vacuum pump through a porous sponge.[1] It is thought that it effectively accelerates wound healing, at least in part by subjecting the wound surface to mechanical forces that promote angiogenesis, nerve regeneration, and the proliferation of cells in the wound.[2–4] However, the contact between the wound and the sponge means that negative-pressure wound therapy increases the risk of infection and pain.[5]

Another mechanotherapeutic approach to wound healing that is widely used in the field is

From the Departments of Plastic, Reconstructive, and Aesthetic Surgery and Pharmacology, Nippon Medical School; and the Department of R&D, Pixie Dust Technologies.
Received for publication November 17, 2018; accepted June 18, 2019.
Presented at the 27th Research Council Meeting of Japan Society of Plastic and Reconstructive Surgery, in Tokyo, Japan, October 19, 2018; and the 48th Annual Meeting of the Japanese Society for Wound Healing, in Tokyo, Japan, November 29, 2018.

DOI: 10.1097/PRS.0000000000006481

Disclosure: *The authors have no conflict of interest to disclose.*

Related digital media are available in the full-text version of the article on www.PRSJournal.com.

the use of ultrasonic waves. At present, three types of ultrasound-based devices have been developed to manage wounds in the clinic, namely, contact high-frequency shock-wave ultrasound devices,[6,7] contact high-frequency focused ultrasound devices, and noncontact low-frequency ultrasound devices. High-frequency shock-wave therapy has been used in the clinic for the past 10 years to induce early tissue repair.[8–11] The contact high-frequency focused ultrasound device is a phased-array device, namely, it consists of an array of ultrasound transducer units that produce ultrasound waves with phase delays. Both of these contact high-frequency devices associate with thermal damage and pain and the consequent distress of the patient. They are also associated with an increased risk of infection. With regard to noncontact low-frequency ultrasound devices, the most well-known is MIST (Celleration Inc., Eden Prairie, Minn.), which consists of a transducer wand and an applicator that produces a saline mist through which the ultrasonic waves pass.[12,13] Other devices use a gel interface. Like the contact devices, these noncontact devices also increase the risk of infection.

To overcome these issues, we developed a noncontact low-frequency ultrasound device that induces wound microdeformation and thereby accelerates healing by delivering high-intensity mechanical force by means of phased-array technology (noncontact low-frequency ultrasound phased-array) without any contact. In the present preclinical study, we asked whether noncontact low-frequency ultrasound phased-array therapy improves acute wound healing. First, we identified the radiation parameters by which our device most reliably induced a homogenous hollow point in extracellular matrix–mimicking hydrogel when it was held at a substantial distance away. Thereafter, we generated acute cutaneous wounds in mice and assessed the effect of applying our device on wound closure and maturation. To determine the underlying mechanisms by which noncontact low-frequency ultrasound phased-array therapy improved wound healing, we also assessed the effect of treatment on epithelialization, angiogenesis (including angiogenesis-related gene signaling), and collagen accumulation.

MATERIALS AND METHODS

Radiation Optimization

The methods used to identify the optimal radiation parameters of our device for inducing microdeformation in cutaneous wounds are described in supplemental digital content.

Animals

All animal experiments were performed according to the guidelines prescribed by the Animal Care and Use Committee of Nippon Medical School. The protocol was approved by the Animal Experiments Ethical Review Committee of Nippon Medical School (approval number 28-011). Male C57BL/6J mice (8 to 9 weeks old; average weight, 25.0 ± 5.0 g) from Charles River Laboratories International (Yokohama, Japan) were used in all animal experiments. Mice were housed individually in temperature- and humidity-controlled vivaria. Mice were allowed to adapt to their vivarium for 1 week before experiments began. In total, 102 mice were used in this study.

Generation of the Wound-Healing Model and Noncontact Low-Frequency Ultrasound Phased-Array Treatment

Mice were anesthetized with 1.5 to 2% isoflurane and their dorsal skin was shaved. On each mouse, a 6-mm-diameter inked tube was stamped twice, once on the left and once on the right of the dorsal midline, to mark the margins of two round 6-mm-diameter full-thickness wounds that were then generated under a microscope with microscissors. The wounds were 1 cm apart. The wounds were subsequently stented as described previously to minimize skin contracture and ensure healing by secondary intention.[14,15] Briefly, an 8-mm-diameter silicone stent was sutured to each wound using 5-0 silk (Natume, Tokyo, Japan). Before the first treatment, both wounds were covered with an adhesive 7-μm film dressing (Skinix Airwall, MA-E5050; Kyowa, Tokyo, Japan) to protect the wound. This dressing was used because of its thinness and its ability to release water vapor: this prevents excessive dryness in the wound. On each mouse, the right and left wounds underwent noncontact low-frequency ultrasound phased-array stimulation and sham treatment, respectively. The treatments were applied for 3 consecutive days starting immediately after wounding (days 0, 1, and 2). Briefly, the ultrasound phased-array transducer was held 160 mm above the surface of the wound.[16] No coupler gels were used. The transducer then generated 5.1 W/cm^{-2} irradiation with a wavelength of 40 kHz ultrasound and a 10-Hz pulse frequency for 60 minutes. For the sham-treated control wounds, the transducer was applied but not activated. After each of the next

two treatments, the dressing was removed from both wounds and new dressings were placed.

Macroscopic Analysis of the Wounds

On days 0, 2, 5, 7, 9, and 14, the wound edges were traced on a transparent polypropylene sheet. The wounds were also photographed with a DMC-GF7W camera (Panasonic Corp., Osaka, Japan) on the same days. The tracings and ImageJ software (National Institutes of Health, Bethesda, Md.) were used to determine the degree of epithelization, which was defined as the epithelialized area divided by the total area of the wound on day 0.

Histologic Analyses of the Wounds

Mice were killed by continuous isoflurane inhalation on postoperative days 2 (immediately after the second treatment/sham treatment), 5, 7, and 14, and their wounds were excised, fixed with 4% paraformaldehyde, embedded in O.C.T. compound (Sakura Finetek, Tokyo, Japan), and frozen with dry ice in acetone. Frozen tissue sections (20-μm thick) were cut vertically from the central region of the wound. Sections were then dried with a dryer for 2 hours. To observe the wound-healing process, five to six sections per wound were stained with hematoxylin and eosin. To semiquantify collagen production, five to six sections per wound were also stained with Masson-trichrome stain as described previously.[17,18] This staining procedure displays the light-green mature collagen and the hematoxylin-purple cell nucleus. All stained sections were then photographed at 4× magnification using a high-resolution camera (DP-74; Olympus). Images were analyzed using imaging software (cellSens; Olympus). All imaging analyses were performed in a double-blinded manner (i.e., sections were photographed and analyzed by two researchers who were blinded in terms of treatment). The density of the collagen in the wound was quantified by measuring the total collagen-stained area and dividing it by the total wound area. The thickness of each granulated wound (from the dorsal muscle fascia to its uppermost surface) was also measured using a low-power field at 4× objective (UPlanFl 0.13 NA).

Immunohistochemical Analysis of Wound Angiogenesis

CD31 is a marker of angiogenesis.[14] To measure the vascular density in wounds, 10-μm-thick frozen sections of the day 2, 5, 7, and 14 wounds were prepared as described above for histologic analyses, then dried for 2 hours, fixed with 4% paraformaldehyde, blocked with 0.1 M phosphate-buffered saline containing 1% normal goat serum at 25°C, and stained for 2 hours at 25°C with anti-CD31 antibody (Purified Rat Anti-mouse CD31, Mec13.3; BD Pharmingen, Franklin Lakes, N.J.) diluted 1:100 in 5% donkey serum. Primary antibody binding was visualized by incubating the section for 1 hour at room temperature with the secondary antibody, Alexa Fluor 488 (Thermo Fisher Scientific K.K., Tokyo, Japan), diluted 1:1000 in 0.1 M phosphate-buffered saline. For 3,3′-diaminobenzidine staining, the section was incubated for 2 hours with biotinylated secondary antibodies, followed by incubation with DAB Substrate (Takara Bio, Inc., Tokyo, Japan). Counterstaining was performed with Mayer's hematoxylin. These stained images were analyzed as described above for the histologic images.

Quantitative Polymerase Chain Reaction

On days, 2, 5, and 7, a wound sample was excised under the microscope and immediately frozen with liquid nitrogen. Total RNA was extracted using RNAiso Plus (Takara Bio). RNA quantification was performed using NanoDrop One (Thermo Fisher Scientific K.K.). Total RNA (400 ng) was reverse-transcribed with a random primer using an iScript Select cDNA Synthesis kit (Bio-Rad Laboratories, Hercules, Calif.). Quantitative polymerase chain reaction was performed using TaqMan Gene Expression Master Mix and the premixed gene-specific TaqMan probe and primer pair (Thermo Fisher Scientific K.K.). (**See Figure, Supplemental Digital Content 1,** which shows a list of the Notch signaling pathway members and the assay identification numbers of the quantitative polymerase chain reaction kits that were used to measure Notch signaling during wound healing, ***http://links.lww.com/PRS/D898***.) Relative expression was analyzed using the $2^{-\Delta\Delta Ct}$ method.

Statistical Analyses

All quantitative macroscopic, histopathologic, and polymerase chain reaction values were expressed as mean ± SD. The Wilcoxon *t* test was used for pairwise comparisons. Statistical significance was defined as a value of $p < 0.05$. All statistical analyses were performed using IBM SPSS Version 18 (IBM Corp., Armonk, N.Y.).

RESULTS

Optimal Irradiation Parameters of Our Noncontact Low-Frequency Ultrasound Device

We first identified the optimal wound irradiation parameters of our original airborne

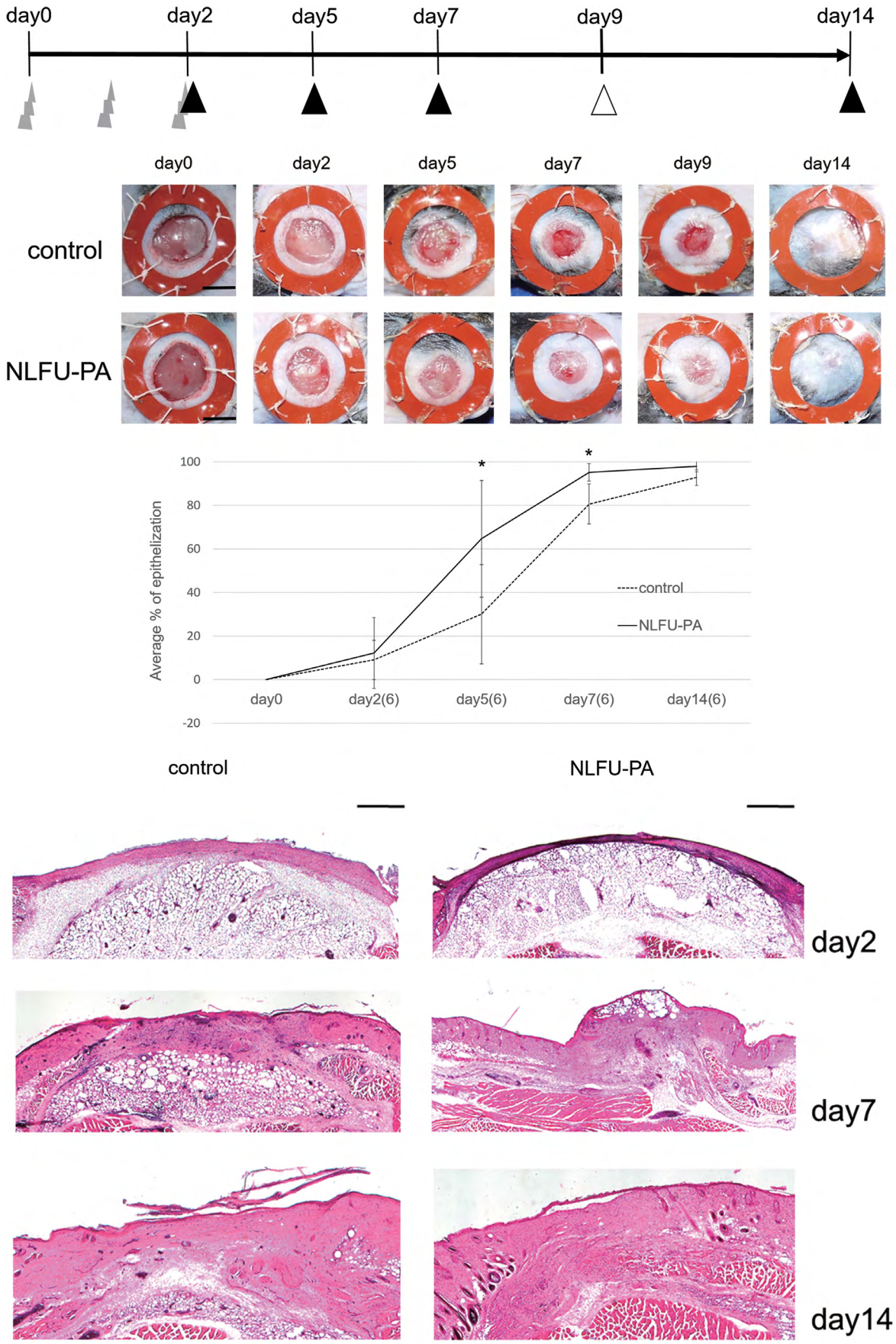

Fig. 1. ***(Continued)***

noncontact low-frequency ultrasound phased-array device[16] by generating gelatin- and sodium hyaluronate–based hydrogels that mimic extracellular matrix and treating different area sizes with the device at a variety of distances and/or pulse frequencies. Our screening analysis with pressure-sensitive fluorescent imaging showed that our device produced a homogeneous hollow point in a 6-mm-diameter area of the hydrogel when the transducer was held 160 mm above the focus point and a pulse frequency of 10 Hz was used. The output force was 16 mN (measured) and then the stimulation pressure was approximately 90.6 Pa (calculated). Thus, our device provides high power (5.1 W/cm^2) despite being held at a substantial distance from the wound (160 mm). Monitoring with a noncontact visual infrared thermometer showed that our device does not exert a thermal effect (<0.4 kW/cm^2). [**See Figure, Supplemental Digital Content 2,** which shows acoustic waves generated by noncontact low-frequency ultrasonic compression generated with phased-array technology and identification of the optimal irradiation parameters. (Above) Two-dimensional schematic depiction of the acoustic waves generated by the noncontact low-frequency ultrasound phased-array device. The wavelets represent ultrasound waves that are emitted by each transducer with delayed excitation. The associated waves are phased near the focal point. The total output force at the focal point is 16 mN. The spatial resolution is 15 mm. (Center) Extracellular matrix-mimicking hydrogels composed of gelatin and sodium hyaluronate (Zhang T, Yan Y, Wang X, et al. Three-dimensional gelatin and gelatin/hyaluronan hydrogel structures for traumatic brain injury. J Bioact Compat Polym. 2007;22:19–29) were loaded with calcein AM (Sigma-Aldrich, St. Louis, Mo.) and mounted on the stage of an inverted microscope. Noncontact ultrasonic irradiation of 16 mN at a pulse frequency of 10 Hz was applied at a height of 160 mm to yield a homogenous hollow point in a 6 mm-diameter area of the hydrogel. A representative image of six experiments is shown. Fluorescence of the calcein AM (excitation, 480 nm; emission, 510 nm) was observed in real-time on the stage of an inverted microscope (FV-3000; Olympus, Tokyo, Japan) with a 1.25× objective (PlanApo 0.04 NA; Olympus). (Below) Analysis of the temperature distribution on the murine wound surface during noncontact low-frequency ultrasound phased-array irradiation for 60 minutes. Thermography (VT02; Fluke, Everett, Wash.) showed that the ultrasound irradiation did not increase the temperature of the wound. The pseudo-color temperature distribution image displays the temperature in degrees Celsius. A representative image of six experiments is shown, ***http://links.lww.com/PRS/D899***.][19]

Fig. 1. Details of the murine wounding and treatment protocol and quantification of epithelialization. (*Above*) Schematic depiction of the treatment protocol. The *gray lightning symbols* indicate when noncontact low-frequency ultrasound phased-array (*NLFU-PA*) treatment was performed. The *arrowheads* indicate when the wound was photographed macroscopically (*black* and *white arrowheads*) and/or subjected to histopathologic evaluation (*black arrowheads*). (*Second row*) Macroscopic view of the treated and sham-treated wounds. Representative images of six mice are shown. This experiment was repeated twice. Similar results were obtained. *Scale bar* = 5 mm. (*Third row*) Degree of wound epithelialization. The data of six mice per time point are expressed as mean and standard deviation. This experiment was repeated twice. Similar results were obtained. (*Below*) Hematoxylin and eosin–stained sections of the sham-treated (*below*, *left*) and noncontact low-frequency ultrasound phased-array–treated wounds (*below*, *right*) on days 2 (the inflammatory phase), 7 (the proliferative phase), and 14 (the mature phase). Representative images of five or six mice (the numbers are shown in parentheses on the *x* axis) per time point are shown. This experiment was repeated four times. Similar results were obtained. *Scale bar* = 500 μm.

Noncontact Low-Frequency Ultrasound Phased-Array Accelerated Acute Wound Epithelialization

To determine the effect of our noncontact low-frequency ultrasound phased-array device on wound healing, we subjected a commonly used murine model of wound healing to treatment at the parameters established by the hydrogel experiments. Thus, two round 6-mm-diameter wounds were generated on either side of the dorsal midline, and the right wound was treated with noncontact low-frequency ultrasound phased-array for 60 minutes/day for 3 consecutive days, starting immediately after wounding. The left wound was sham-treated (control) with the device on the same days (Fig. 1, *above*). Macroscopic analyses showed how the raw wounds (red with an exudate) epithelialized (light pink and dry surfaces) over time. The treatment significantly accelerated wound closure, which was defined as full epithelialization over the granulated tissue from the wound edge. Thus, the treated wound showed significant wound closure on day 5. By contrast, the sham-treated wound only reached that stage 1 to 2 days later (Fig. 1, *second row*). Indeed, ImageJ software analysis of the wounds showed that on day 5, 65 ± 27 percent and 30 ± 23 percent of the total

(day 0) treated and sham-treated wound surfaces had epithelialized, respectively ($p < 0.05$). Similarly, on day 7, 95 ± 4 percent and 81 ± 9 percent of the treated and sham-treated wound surfaces had epithelialized, respectively ($p < 0.05$) (Fig. 1, *third row*).

The mice were killed on days 2, 5, 7, and 14 and their wounds were subjected to histologic evaluation. Hematoxylin and eosin staining indicated the degree of inflammatory cell infiltration of the wound bed along with the degree of epithelialization. This shows the progression of the three phases of wound healing (i.e., inflammatory, proliferative, and maturation phases) (Fig. 1, *below*). The treated wounds were more advanced at all three phases of wound healing than the sham-treated wounds. Specifically, although both wounds contained inflammatory cells on day 2, there were fewer inflammatory cells in the treated wounds on day 7. Moreover, the treated wounds exhibited complete epithelialization on day 14, unlike the sham-treated wounds (Fig. 1, *below*).

Noncontact Low-Frequency Ultrasound Phased-Array Treatment Enhanced Early Angiogenesis

When we subjected the murine wounds to immunohistochemistry with anti-CD31 antibody, we found that the treated wounds exhibited enhanced neovascularization at all time points (days 2, 5, 7, and 14) (Fig. 2, *above*). Indeed, image analysis showed that on day 2, the treated wounds had significantly larger $CD31^+$ areas relative to total wound area (4.6 ± 1.7 percent) than the sham-treated wounds (2.2 ± 1.0 percent) ($p < 0.05$). This disparity was also observed on days 5 (9.9 ± 2.8 percent versus 6.5 ± 2.7 percent), 7 (7.3 ± 3.5 percent versus 4.7 ± 2.9 percent), and 14 (2.6 ± 0.7 percent versus 1.5 ± 0.8 percent) (all $p < 0.05$) (Fig. 2, *below*). To determine where CD31 localizes in the treated wounds, the $CD31^+$ area in a noncontact low-frequency ultrasound–treated wound on day 5 was first identified. Thereafter, we performed immunogold-labeling microscopy on ultrathin sections of the $CD31^+$ areas of this day-5 wound. We observed that the endothelial cells stained more intensely with anti-CD31 antibody than the other cell types. [**See Figure, Supplemental Digital Content 3,** which shows (above) the CD31+ area in the immunohistochemistry-stained section of the noncontact low-frequency ultrasound–treated wound on day 5. Scale bar = 500 μm. (Below) Immunoelectron microscopic analysis of wound angiogenesis. Low-power (below, left) and high-power (below, right) views of the immunogold-labeled microscope image. N, nucleus of the endothelial cell; P, pericyte. Black dots delineated by white dashes indicate the CD31+ cytoplasm of the endothelial cells. Representative images of five ultrathin sections from one noncontact low-frequency ultrasound–treated wound are shown. Scale bars = 5 μm in the left image and 500 nm in the right image. Wound angiogenesis was assessed by immunoelectron microscopic analysis as described previously (Brandstaetter H, Kishi-Itakura C, Tumbarello DA, Manstein DJ, Buss F. Loss of functional MYO1C/myosin 1c, a motor protein involved in lipid raft trafficking, disrupts autophagosome-lysosome fusion. Autophagy 2014;10:2310–2323). Briefly, the preembedding gold enhancement immunogold method was performed on semithin sections that were prepared in the same way as the specimens for histologic analyses. The sections were washed with 0.1 M phosphate-buffered saline and blocked for 30 minutes at room temperature by immersion in a droplet of 0.1 M phosphate-buffered saline containing 1% bovine serum albumin and 0.1% saponin. Thereafter, the sections were placed in a droplet of 0.1 M phosphate-buffered saline containing rat anti-CD31 antibody (BD Pharmingen, diluted 1:100) for 24 hours at 4°C. After washing with 0.1 M phosphate-buffered saline, the sections were incubated for 2 hours at room temperature with 1.4 nm nanogold colloidal particles diluted 1:20 (Nanoprobes, Yaphank, N.Y.) in a solution consisting of 0.1 M phosphate-buffered saline containing 1% bovine serum albumin and 0.1% saponin. They were then washed with 0.1 M phosphate-buffered saline, fixed with 1% glutaraldehyde in 0.1 M phosphate-buffered saline for 10 minutes, washed with water, treated with gold enhancement (Nanoprobes), washed again with water, and then fixed with 1% osmium tetroxide in 0.1 M phosphate-buffered saline. Finally, the sections were dehydrated with a graded series of ethanol and embedded in Epon 812 (Polysciences, Inc., Warrington, Pa.). The ultrathin sections were then mounted on copper grids, stained with uranyl acetate, and examined by transmission electron microscopy (JEM-1400 plus; JEOL, Tokyo, Japan), ***http://links.lww.com/PRS/D900***.][20]

Noncontact Low-Frequency Ultrasound Phased-Array Facilitated Collagen Production in the Acute Wound

To observe collagen production, we subjected the sections from the day 0, 2, 5, 7, and 14 noncontact low-frequency ultrasound–treated and

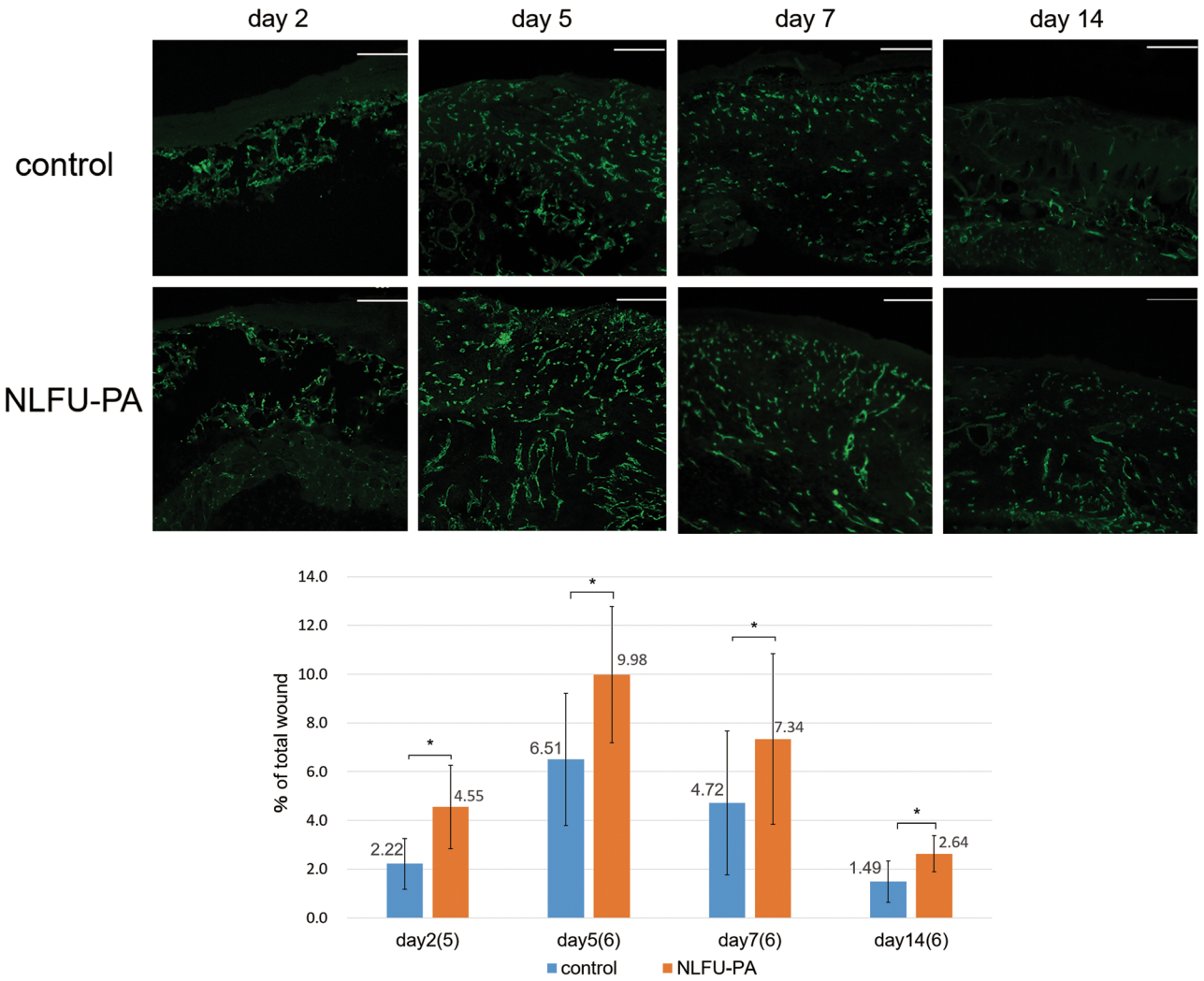

Fig. 2. Quantification of angiogenesis. (*Above*) Immunohistochemical analysis of CD31 expression. Representative images of five or six mice (the numbers are shown in parentheses) per time point are shown. *Scale bar* = 200 μm. (*Below*) Percentage of area that is CD31⁺. The data of five or six mice (the numbers are shown in parentheses on the *x* axis) per time point are expressed as mean and standard deviation. This experiment was repeated three times. Similar results were obtained. *$p < 0.05$, as determined by the Wilcoxon *t* test. *NLFU-PA*, noncontact low-frequency ultrasound phased-array.

sham-treated wounds to Masson-trichrome staining and low-power photography (Fig. 3, *above*). Image analysis then served to measure the density of collagen in the tissue above the muscle fascia. Relative to the total area of the wound, the treated wounds had significantly greater collagen density (44 ± 14 percent) than the sham-treated wounds (28 ± 13 percent) on day 5 ($p < 0.05$). This significant difference was also observed on days 7 (53 ± 12 percent versus 38 ± 19 percent) and 14 (52 ± 12 percent versus 39 ± 7 percent) (both $p < 0.05$) (Fig. 3, *second row*). Moreover, when the thickness of the granulated tissue in the wounds was measured (i.e., from the dorsal muscle fascia to the top of the wound surface), the treated wounds had significantly thicker granulated tissue than the sham-treated wounds on days 5 (740 ± 310 μm versus 520 ± 250 μm) and 14 (990 ± 170 μm versus 540 ± 160 μm) (both $p < 0.05$) (Fig. 3, *third row* and *below*).

Involvement of the Notch Signaling Pathway

To elucidate the mechanisms underlying the beneficial effect of our device, we examined the effect of noncontact low-frequency ultrasound phased-array on Notch signaling. Therefore, we assessed the mRNA expression of EphB2,[21] Notch1/3,[22] Hey1/2,[23,24] delta-like 1 protein (Dll) 1/4,[24] Jag1/2,[25] EphB4,[21] and two relevant transcription factors, Myt and Hes5[23,24] (**see Figure,**

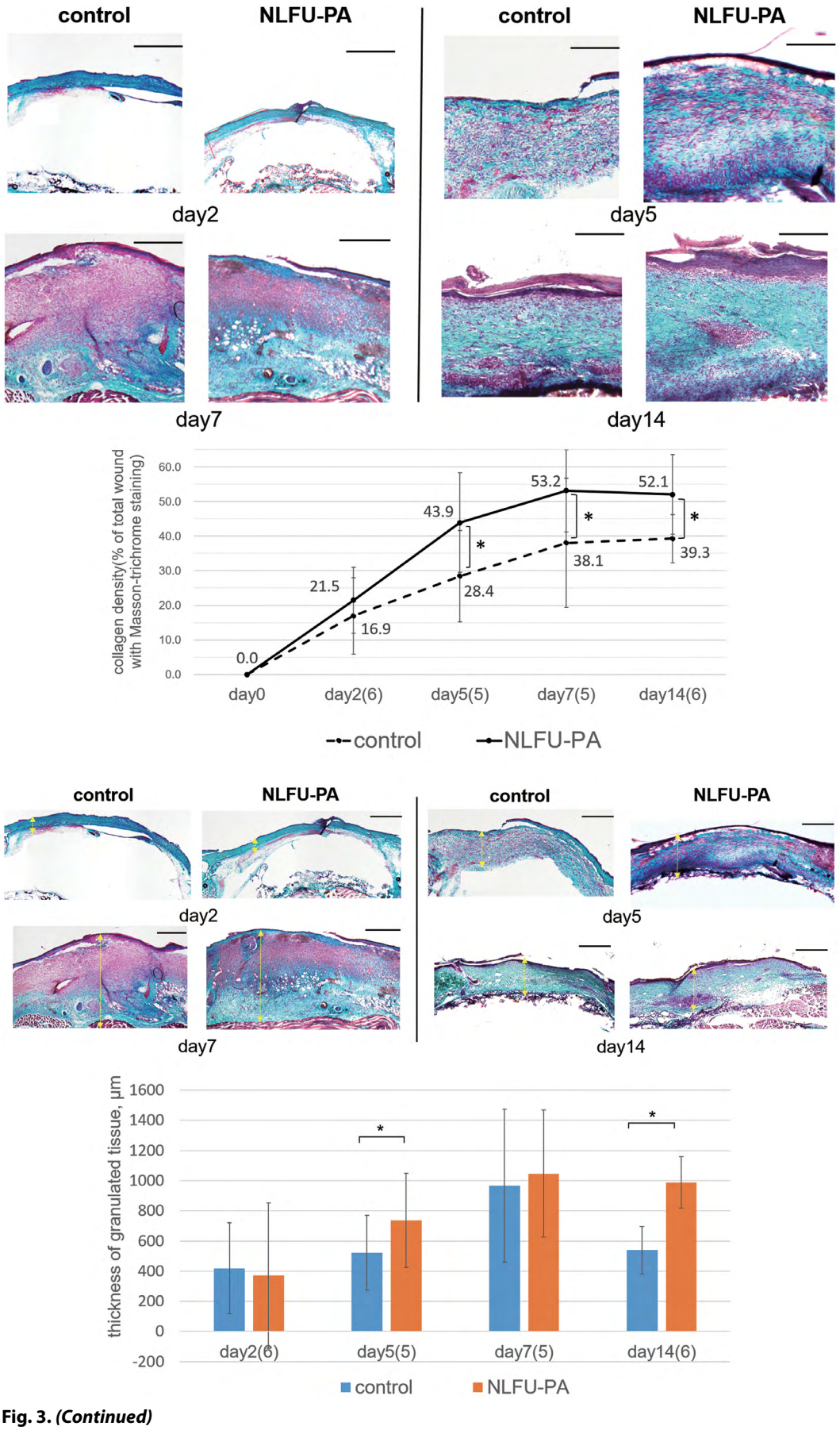

Fig. 3. ***(Continued)***

Supplemental Digital Content 1, *http://links.lww.com/PRS/D898*).

We found that, compared with sham treatment, noncontact low-frequency ultrasound phased-array treatment significantly elevated the expression of Dll1 on days 2 (160 ± 72 percent versus 100 ± 89 percent) and 5 (180 ± 72 percent versus 100 ± 110 percent) (both $p < 0.05$) (Fig. 4, *above* and *center*). Treatment also significantly increased Notch1 expression on day 5 (190 ± 68 percent versus 100 ± 58 percent) ($p < 0.05$) (Fig. 4, *center*). These treatment-induced temporal changes are consistent with the treatment-induced changes in angiogenesis, as observed by our histologic analyses (Fig. 2).

DISCUSSION

Our noncontact low-frequency ultrasound phased-array device significantly accelerated wound closure and maturation. This was associated with an early rise in angiogenesis that was followed later by amplified epithelialization and collagen production. We also analyzed the expression of several angiogenesis-related genes to elucidate the possible biological mechanisms by which our device accelerates wound healing. We observed that the device significantly increased the transient expression of Dll1 and Notch1 soon after starting noncontact low-frequency ultrasound phased-array treatment. Dll1 was expressed first, which suggests that it drove Notch1 expression. The temporal association of these changes with early angiogenesis suggests that these genes drive the beneficial effects of noncontact low-frequency ultrasound phased-array treatment.

Fig. 3. Quantification of collagen production. (*Above* and *third row*) The sham-treated and treated wounds were sectioned and treated with Masson trichrome stain. High-power (*above*) and low-power (*third row*) views of the sham-treated (*left images*) and treated (*right images*) wounds on days 2 (*above*, *left images*), 5 (*above*, *right images*), 7 (*below*, *left images*), and 14 (*below*, *right images*). Representative images of five or six mice (the numbers are shown in parentheses on the *x* axis) per time point are shown. This experiment was repeated three times. Similar results were obtained. *Scale bars* = 200 μm (*above*) and 500 μm (*third row*). (*Second row* and *below*) Density of collagen tissue relative to the total wound area (*second row*) and the thickness of granulation tissue (*below*) in the wounds. The data of five or six mice per time point are expressed as mean and standard deviation. This experiment was repeated three times. Similar results were obtained. *$p < 0.05$, as determined by the Wilcoxon *t* test. *NLFU-PA*, noncontact low-frequency ultrasound phased-array.

Several innovative and potential therapeutic devices such as MIST[12,13] and those that provide negative-pressure wound therapy[2–4] and extracorporeal shock-wave therapy[8–11] accelerate wound healing by placing mechanical pressure on the wound surface and thereby inducing tissue microdeformation. All existing devices of this nature use direct contact or an aqueous gel or water as the coupling medium. The pressure induces hydrodynamic cavitation and acoustic microstreaming; these effects cause the cells in the wound to express angiogenesis-related genes. As a result, these devices induce neovascularization,[4,8,10,13] which is a crucial early step in wound healing.

Noncontact low-frequency ultrasound phased-array treatment is noninvasive, does not involve direct contact with the wound, does not require any coupling medium, and is relatively simple to set up and use relative to the conventional devices. In the literature, the maximum intensity of existing noncontact low-frequency ultrasound devices is 3 W/cm^{-2}.[10] Despite the fact that it is a high-intensity device, our device does not induce any heat and is therefore likely to be painless. Most importantly, we provided the first evidence showing that this device significantly accelerated the closure of acute murine wounds, and that this benefit was associated with a potent and early up-regulation of angiogenesis. Endothelial cells play a crucial role in wound healing because the microvasculature they produce not only maintains systemic homeostasis, it also mediates the evolution of immune responses after wounding and the subsequent proliferative and maturation phases of wound healing.[26] Our data are consistent with the fact that wound healing in mice is associated with angiogenesis signaling on days 3 and 5 after wounding.[26] We also observed that our device amplified collagen proliferation. It is likely that this is secondary to the early effect of the device on angiogenesis. This is supported by Maan et al., who reported that noncontact low-frequency ultrasound treatment involving a saline mist improves wound healing and that this associates not only with greater collagen deposition but also higher expression of angiogenic cytokines such as vascular endothelial growth factor.[13] We also found that noncontact low-frequency ultrasound phased-array treatment may promote early angiogenesis through the rapid transient increase of first Dll1 and then Notch1 activation. Notch signaling plays an important role in wound angiogenesis: several studies show that it regulates wound healing, including the repair of the epidermal barrier

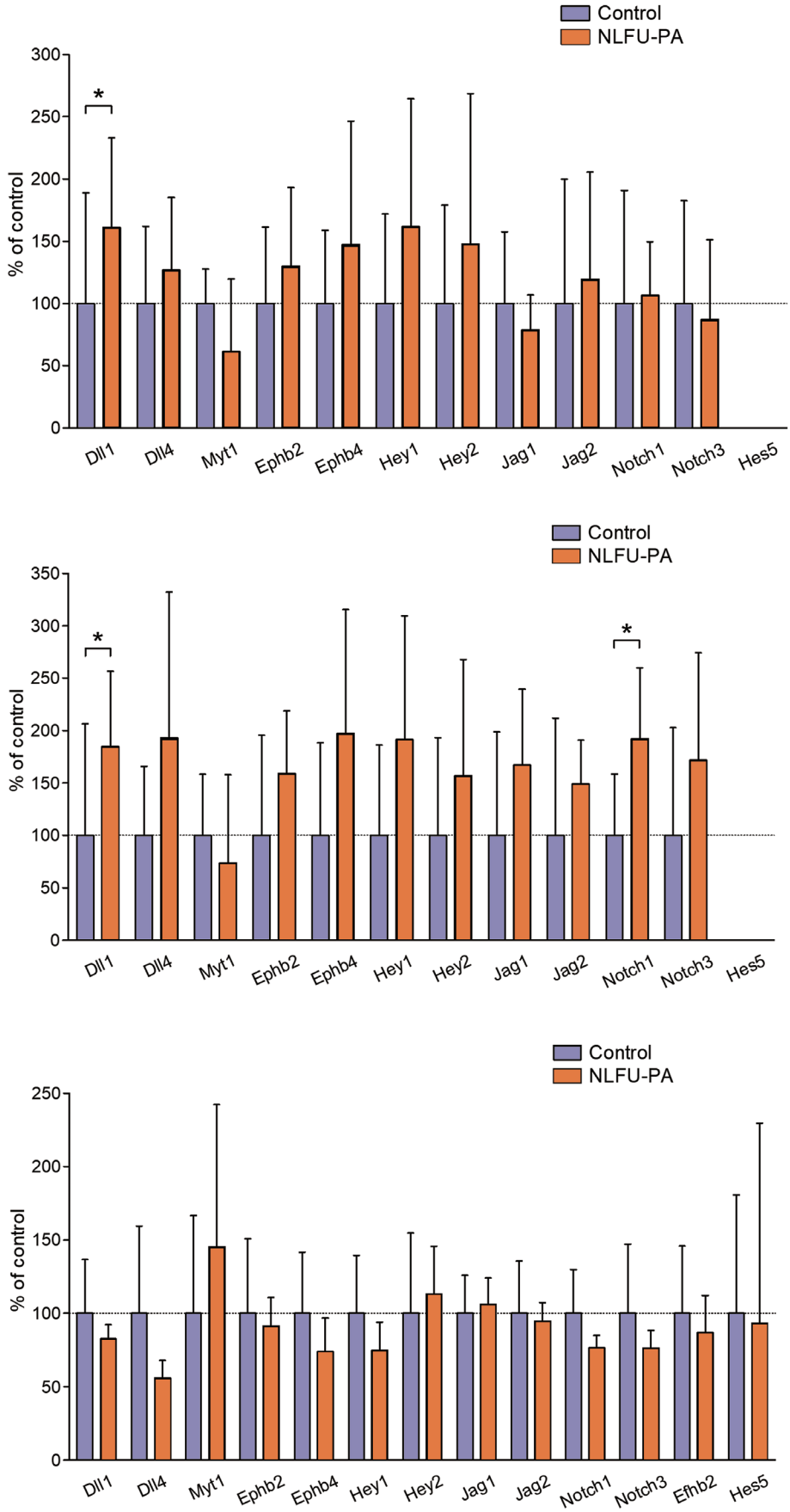

Fig. 4. ***(Continued)***

and the dermis, and that this activity is associated with the production of proangiogenic factors by the wound.[27] In addition, Notch plays essential physiologic functions in the development of the circulatory system, including the blood vessels,[27] and has been implicated in postnatal angiogenesis.[22] It has been shown that shear stress elevates the transcription of several Notch-related arterial endothelial cell markers,[28] namely, Notch1/3 and the Notch ligands Dll1/4, and the expression of the Notch-related venous endothelial cell marker EphB4.[21] The fact that Dll1 was up-regulated before angiogenesis is consistent with Sörensen et al., who showed that Dll1 is crucial for Notch1 activation in fetal arterial endothelial cells.[29] Thus, a Dll1/Notch1 signaling pathway may mediate the positive effect of our device on acute wound healing. This is supported by Patel et al., who showed that the lack of Notch signaling causes excessive fibrosis in wounds and that this results in delayed wound healing.[30]

CONCLUSIONS

In conclusion, our findings suggest that noncontact low-frequency ultrasound phased-array treatment may exert its clinical effects on acute wounds by up-regulating first Dll1 and then Notch1, which in turn initiate important wound-healing processes, specifically, early angiogenesis. Further studies assessing the effect of noncontact low-frequency ultrasound phased-array treatment on delayed wound healing in diabetic mice and other models of pathologic wound healing are warranted. In addition, studies that examine how the mechanical stress provided by our device and others activates mechanosensors and induces molecular mechanosignaling are needed. Moreover, studies that compare our device to existing therapies in terms of pain and infection rates will be valuable. These studies with our device are likely to expand the field of mechanotherapeutic proangiogenesis, thereby helping to bring about a new revolution in the care of not only chronic wounds but also acute wounds.

Fig. 4. Notch signaling during wound healing. The mRNA expression of genes involved in the Notch signaling pathway was measured in the treated and sham-treated wounds on days 2 (*above*), 5 (*center*), and 7 (*below*) using quantitative polymerase chain reaction. The treated wound data are expressed relative to the sham-treated wound data, which were set at 100 percent. The data of five or six mice per time point are expressed as mean and standard deviation. This experiment was repeated four times. Similar results were obtained. *$p < 0.05$, as determined by the Wilcoxon *t* test. *NLFU-PA*, noncontact low-frequency ultrasound phased-array.

Hiroya Takada, Ph.D.
Department of Plastic, Reconstructive, and Aesthetic Surgery
Nippon Medical School
1-1-5 Sendagi, Bunkyo-ku
Tokyo 113-8602, Japan
h-takada@nms.ac.jp

REFERENCES

1. Argenta LC, Morykwas MJ, inventors. Wake Forest University, assignee. Method of treating tissue damage and apparatus for same. U.S. Patent 5645081. July 8, 1997.
2. Saxena V, Hwang CW, Huang S, Eichbaum Q, Ingber D, Orgill DP. Vacuum-assisted closure: Microdeformations of wounds and cell proliferation. *Plast Reconstr Surg.* 2004;114:1086–1096; discussion 1097–1098.
3. Younan G, Ogawa R, Ramirez M, Helm D, Dastouri P, Orgill DP. Analysis of nerve and neuropeptide patterns in vacuum-assisted closure-treated diabetic murine wounds. *Plast Reconstr Surg.* 2010;126:87–96.
4. Erba P, Ogawa R, Ackermann M, et al. Angiogenesis in wounds treated by microdeformational wound therapy. *Ann Surg.* 2011;253:402–409.
5. Sowa Y, Numajiri T, Uenaka M, Itsukage S, Sugimoto K, Nishino K. Clinical experience of wound treatment using negative pressure wound therapy (NPWT): A study of 40 cases. *J Kyoto Pref Univ Med.* 2011;120:243–251.
6. Yang G, Luo C, Yan X, Cheng L, Chai Y. Extracorporeal shock wave treatment improves incisional wound healing in diabetic rats. *Tohoku J Exp Med.* 2011;225:285–292.
7. Zissler A, Stoiber W, Pittner S, Sänger AM. Extracorporeal shock wave therapy in acute injury care: A systematic review. *Rehabil Process Outcome* 2018;7:1–13.
8. Qureshi AA, Ross KM, Ogawa R, Orgill DP. Shock wave therapy in wound healing. *Plast Reconstr Surg.* 2011;128:721e–727e.
9. Huang C, Holfeld J, Schaden W, Orgill D, Ogawa R. Mechanotherapy: Revisiting physical therapy and recruiting mechanobiology for a new era in medicine. *Trends Mol Med.* 2013;19:555–564.
10. Hatanaka K, Ito K, Shindo T, et al. Molecular mechanisms of the angiogenic effects of low-energy shock wave therapy: Roles of mechanotransduction. *Am J Physiol Cell Physiol.* 2016;311:C378–C385.
11. d'Agostino MC, Craig K, Tibalt E, Respizzi S. Shock wave as biological therapeutic tool: From mechanical stimulation to recovery and healing, through mechanotransduction. *Int J Surg.* 2015;24:147–153.
12. Sussman C, Dyson M. Therapeutic and diagnostic ultrasound. In: Sussman C, Bates-Jensen B, eds. *Wound Care: A Collaborative Practice Manual for Health Professionals.* Philadelphia: Wolters Kluwer Health/Lippincott Williams & Wilkins; 2007:684–726.
13. Maan ZN, Januszyk M, Rennert RC, et al. Noncontact, low-frequency ultrasound therapy enhances neovascularization and wound healing in diabetic mice. *Plast Reconstr Surg.* 2014;134:402e–411e.
14. Matsumoto S, Tanaka R, Okada K, et al. The effect of control-released basic fibroblast growth factor in wound healing: Histological analyses and clinical application. *Plast Reconstr Surg Glob Open* 2013;1:e44.
15. Galiano RD, Michaels J V, Dobryansky M, Levine JP, Gurtner GC. Quantitative and reproducible murine

model of excisional wound healing. *Wound Repair Regen.* 2004;12:485–492.
16. Hoshi T, Takahashi M, Iwamoto T, Shinoda H. Noncontact tactile display based on radiation pressure of airborne ultrasound. *IEEE Trans Haptics* 2010;3:155–165.
17. Huang H, Zhang Q, Liu J, Hao H, Jiang C, Han W. Granulocyte-colony stimulating factor (G-CSF) accelerates wound healing in hemorrhagic shock rats by enhancing angiogenesis and attenuating apoptosis. *Med Sci Monit.* 2017;23:2644–2653.
18. Jimi S, Kimura M, De Francesco F, Riccio M, Hara S, Ohjimi H. Acceleration mechanisms of skin wound healing by autologous micrograft in mice. *Int J Mol Sci.* 2017;18:1–14.
19. Zhang T, Yan Y, Wang X, et al. Three-dimensional gelatin and gelatin/hyaluronan hydrogel structures for traumatic brain injury. *J Bioact Compat Polym.* 2007;22:19–29.
20. Brandstaetter H, Kishi-Itakura C, Tumbarello DA, Manstein DJ, Buss F. Loss of functional MYO1C/myosin 1c, a motor protein involved in lipid raft trafficking, disrupts autophagosome-lysosome fusion. *Autophagy* 2014;10:2310–2323.
21. Adams RH, Wilkinson GA, Weiss C, et al. Roles of ephrinB ligands and EphB receptors in cardiovascular development: Demarcation of arterial/venous domains, vascular morphogenesis, and sprouting angiogenesis. *Genes Dev.* 1999;13:295–306.
22. Shih YT, Wang MC, Yang TL, et al. β(2)-Integrin and Notch-1 differentially regulate CD34(+)CD31(+) cell plasticity in vascular niches. *Cardiovasc Res.* 2012;96:296–307.
23. Abdolazimi Y, Stojanova Z, Segil N. Selection of cell fate in the organ of Corti involves the integration of Hes/Hey signaling at the Atoh1 promoter. *Development* 2016;143:841–850.
24. Ahnfelt-Rønne J, Hald J, Bødker A, Yassin H, Serup P, Hecksher-Sørensen J. Preservation of proliferating pancreatic progenitor cells by Delta-Notch signaling in the embryonic chicken pancreas. *BMC Dev Biol.* 2007;7:63.
25. Kopan R, Ilagan MX. The canonical Notch signaling pathway: Unfolding the activation mechanism. *Cell* 2009;137:216–233.
26. Shrader CD, Ressetar HG, Luo J, Cilento EV, Reilly FD. Acute stretch promotes endothelial cell proliferation in wounded healing mouse skin. *Arch Dermatol Res.* 2008;300:495–504.
27. Johnson KE, Wilgus TA. Vascular endothelial growth factor and angiogenesis in the regulation of cutaneous wound repair. *Adv Wound Care (New Rochelle)* 2014;3:647–661.
28. Obi S, Yamamoto K, Shimizu N, et al. Fluid shear stress induces arterial differentiation of endothelial progenitor cells. *J Appl Physiol (1985)* 2009;106:203–211.
29. Sörensen I, Adams RH, Gossler A. DLL1-mediated Notch activation regulates endothelial identity in mouse fetal arteries. *Blood* 2009;113:5680–5688.
30. Patel J, Baz B, Wong HY, Lee JS, Khosrotehrani K. Accelerated endothelial to mesenchymal transition increased fibrosis via deleting Notch signaling in wound vasculature. *J Invest Dermatol.* 2018;138:1166–1175.